Meteor Trail Echo Rejection in Atmospheric Phased Array Radars Using Adaptive Sidelobe Cancellation

TAISHI HASHIMOTO

Department of Communications and Computer Engineering, Kyoto University, Kyoto, Japan

KOJI NISHIMURA AND MASAKI TSUTSUMI

National Institute of Polar Research, Tachikawa, Japan

TORU SATO

Department of Communications and Computer Engineering, Kyoto University, Kyoto, Japan

(Manuscript received 6 February 2014, in final form 21 May 2014)

ABSTRACT

Strong meteor trail echoes are interferences in the wind velocity estimates made from mesosphere radar observations. Contaminated spectra are detected by their discontinuity and are removed at the risk of greater fluctuations of spectra, leading to a severe reduction of the signal-to-noise ratio (SNR) and inaccurate wind estimates for weak atmospheric echoes. This paper presents an adaptive signal processing technique for the suppression of spectral contaminations by meteor trail echoes. The method is based on the norm-constrained and directionally constrained minimization of power (NC-DCMP), which balances the capability of canceling the clutter and the robustness of beam shaping, at the cost of a slight decrease in the SNR, which can be determined in advance. Simulation results show that with a 3-dB decrease of the SNR being allowed, the method improves the signal-to-interference ratio (SIR) by 15 dB, giving wind estimates that are about $8 \, \text{m s}^{-1}$ better in terms of root-mean-square error and providing 4 times as wide an observable range when compared with the results of the ordinary nonadaptive beamforming method. The results for an actual observation show that the improvement of both the SIR and the observable range are achieved as in the simulations, which implies that the method should provide the simulated accuracy for the estimation of wind velocity from actual observations.

1. Introduction

In observations of mesosphere wind employing Doppler radars, strong meteor echoes often contaminate spectra. Usually, these spectra with meteor echoes are automatically detected by their discontinuity in time and height, and are discarded before the incoherent integration and wind velocity estimation are made (Tsuda et al. 1985). However, only outstanding echoes can be removed employing this method. Additionally, decreasing the number of spectra for incoherent integration increases the fluctuations of spectra, which introduces estimation errors of the wind velocity of weak mesosphere echoes.

This paper presents an adaptive signal processing technique for reducing interferences from meteor trail echoes in mesosphere wind observations. The base method has been shown to be a good solution for the rejection of interference from the ground (Kamio et al. 2004) and accurate estimation of the vertical wind velocity (Nishimura et al. 2012). However, this is not the case for rapidly moving objects such as aircraft. Meteor trail echoes are also moving objects and have strong echo intensity, but they are relatively slow and the method works well for them.

The contents of this paper are as follows. In section 2, the theory and implementation of the method are stated. Section 3 explains the simulation model and gives the result of applying the adaptive meteor clutter rejection technique to the model. In section 4, we apply the

Corresponding author address: Taishi Hashimoto, Dept. of Communications and Computer Engineering, Kyoto University, Yoshida-Hommachi, Sakyo-ku, Kyoto 606-8501, Japan.
E-mail: thashimoto@sato-lab.0t0.jp

method to an actual observation and show the result. Section 5 summarizes the proposed method and gives conclusions.

2. Methods and implementations

In this section, adaptive signal processing methods and their implementations are stated.

a. Directionally constrained minimization of power

The directionally constrained minimization of power (DCMP) algorithm is an adaptive beamforming algorithm for the special case of known desired directions. According to Takao et al. (1976), the basic theory of DCMP is written as a nonlinear optimization problem:

$$\min_{\mathbf{W}} \left(P_{\text{out}} = \frac{1}{2}\mathbf{W}^H \mathbf{R}_{xx} \mathbf{W} \right) \quad \text{subject to} \quad \mathbf{C}^T \mathbf{W}^* = H, \quad (1)$$

where $(\cdot)^*$ denotes the complex conjugate, $(\cdot)^T$ is for the transposition, and $(\cdot)^H$ is for the adjoint (conjugate transpose) matrix. Assuming M receivers, $\mathbf{R}_{xx} \equiv \mathbf{X}\mathbf{X}^H$ is the covariance matrix of the received signals $\mathbf{X} = [X_1, \ldots, X_M]^T$ and $\mathbf{W}$ is the optimal weight vector. Term $\mathbf{C}$ is called the directional constraint, which is a function of the geometric location of each receiver $\mathbf{L}_i$ ($i = 1, \ldots, M$) and the desired direction (zenith, azimuth) = (θ, ϕ). Using an array manifold function $\mathbf{A}(\theta, \phi)$, C_i can be written as

$$C_i = A_i(\theta, \phi) = \exp\left(\frac{2\pi i}{\lambda}\mathbf{L}_i \cdot \mathbf{V}\right)$$
$$\mathbf{V} = [\sin\theta\cos\phi, \sin\theta\sin\phi, \cos\theta]^T. \quad (2)$$

Term λ is the radar wavelength and H is called the constraint response against each corresponding $\mathbf{C}$; H takes a value from 0 to 1 and determines the null depth or the peak height of the beam pattern in the specific direction defined by $\mathbf{C}$. Term $\mathbf{V}$ is a unit vector to the radial direction (θ, ϕ). The combined outputs of beam synthesis Y is obtained by

$$Y = \mathbf{W}^H \mathbf{X}. \quad (3)$$

b. Norm-constrained DCMP

The norm-constrained DCMP (NC-DCMP) has an additional constraint of the magnitude of the norm of $\mathbf{W}$ in Eq. (1):

$$\mathbf{W}^H \mathbf{W} \le U. \quad (4)$$

Here, U is the norm constraint that preserves the shape of the main lobe even when only an incorrect steering vector is available.
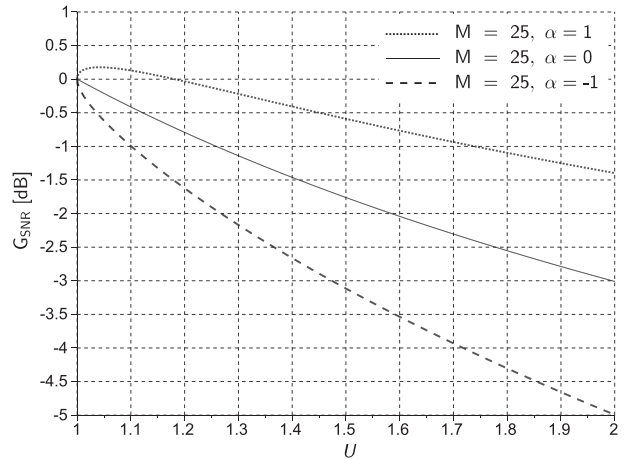
FIG. 1. Relationship between U and G_{SNR} in the 25-channel radar system assuming the MU radar. The abscissa is U and the ordinate is G_{SNR}. Each line corresponds to a different phase rotation: $\alpha = 1$ (in phase; top line), $\alpha = -1$ (opposite phase; bottom line) and $\alpha = 0$ (intermediate; middle line). We use the middle line for deciding U.

For the NC-DCMP algorithm, one can determine U from the permissive loss in the signal-to-noise ratio (SNR). The relationship between the SNR loss G_{SNR} and the norm constraint U is described in Kamio et al. (2004):

$$G_{\text{SNR}} = \frac{\left[1 + \alpha\sqrt{U/(M-1)}\right]^2}{1+U}, \quad (5)$$

where α takes a value from -1 to 1 and represents the phase rotational relation between each channel. Equation $\alpha = 1$ means an in-phase relation, which is obtained employing the ideal beamforming method without availability of clutter rejection. Equation $\alpha = -1$ means an opposite-phase relation, which is the worst case, suppressing the desired signals. Equation $\alpha = 0$ is the intermediate of these two cases and is used to decide the norm constraint U in later sections. Figure 1 is an example of plotting Eq. (5) at each $\alpha = -1, 0, 1$ for $M = 25$, which corresponds to the number of channels of the middle and upper (MU) atmosphere radar.

c. Norm-constrained tamed adaptive antenna

As mentioned above, NC-DCMP requires the solving of a nonlinear optimization problem with an inequality constraint, which severely increases the calculation cost. However, according to Wang et al. (2003), the norm $\mathbf{W}^H \mathbf{W}$ is known to decrease monotonically as β increases and in the special case of the equality of Eq. (4) being satisfied, the solution can be easily obtained as

$$\mathbf{W} = \frac{\hat{\mathbf{R}}_{xx}^{-1}\mathbf{C}}{\mathbf{C}^{H}\hat{\mathbf{R}}_{xx}^{-1}\mathbf{C}}H^{*},$$

$$\hat{\mathbf{R}}_{xx} \equiv \mathbf{R}_{xx} + \beta\mathbf{I}, \tag{6}$$

where $\mathbf{I}$ is a unit matrix and $\beta > 0$ represents the magnitude of the pseudonoise added to the covariance matrix. The solution in Eq. (6) is exactly the same as the optimal weight vector of the tamed adaptive antenna array mentioned in Takao and Kikuma (1986), but β cannot be obtained directly. Thus, β is determined as follows:

(i) Estimate the boundary of the norm constraint U from the permissive SNR loss G_{SNR} using Eq. (5).

(ii) Set $\beta = 0$ and calculate $\mathbf{W}_{\beta=0}$. If Eq. (4) is already satisfied by $\mathbf{W}_{\beta=0}$, then this solution is optimal. Otherwise, continue to the next.

(iii) Find the minimum β that satisfies the equality condition of Eq. (4). This can be effectively calculated employing a one-dimensional root-finding algorithm such as Newton's method.

We call this method, which is an effective way to calculate the optimal weight of NC-DCMP, the norm-constrained tamed adaptive (NC-TA) method in later sections. Depending on the selection of U, the NC-TA method may fail in finding the optimal weight vector $\mathbf{W}$. Thus, in practice, one can start this routine with small U and then iterate by increasing G_{SNR}.

3. Simulation of adaptive meteor clutter rejection

In this section, we show the result of simulations of the adaptive meteor clutter rejection technique for mesospheric radar observations.

a. Generating simulation data of atmospheric and meteor echoes

In this simulation, each spectrum contains two kinds of echoes, atmospheric and meteor echoes. In the following subsections, detailed procedures of generating atmospheric and meteor echoes are stated.

1) ATMOSPHERIC ECHOES

Power spectra of atmospheric echoes returned by backscattering from turbulences are modeled by a Gaussian function as follows (Yamamoto et al. 1988):

$$S_m(v) = \frac{P_S}{\sqrt{2\pi}\sigma}\exp\left[-\frac{(v - v_d)^2}{2\sigma^2}\right] + P_N, \tag{7}$$

where v is the radial wind velocity, P_S is the echo intensity of the atmospheric echo, P_N is the noise floor level, v_d is the mean Doppler velocity of the wind, and σ

is the spectral width. Additionally, the time series of complex outputs at each receiver has random fluctuations following a Gaussian distribution for both real and imaginary components. This results in the model spectrum having the statistical fluctuation following a χ^2 distribution with 2 degrees of freedom, because the power spectra are the squared sum of complex received signals. The model spectrum with these fluctuations, $S'_m(v)$, can now be obtained as the product of $S_m(v)$ and random numbers following a χ^2 distribution with 2 degrees of freedom.

For the adaptive signal processing, we need complex outputs at each receiver $s_i(t)$ ($i = 1, \ldots, M$, where M is the number of receivers). To reproduce these from $S'_m(v)$, we can use the inverse Fourier transform and the array manifold, which is stated in the previous section. First, we perform the inverse Fourier transform to obtain the basic complex outputs at the phase origin, $s_o(t)$, which is a time series:

$$s_o(t) = \mathcal{F}^{-1}\left[\sqrt{S'_m(v)} \angle \rho(v)\right], \tag{8}$$

where $A \angle B$ represents a complex number with its amplitude A and phase B, $\mathcal{F}^{-1}[\cdot]$ stands for the inverse Fourier transform, and $\rho(v)$ is a uniform random-number generator having a range of $[0, 2\pi]$. As shown by Eq. (8), amplitudes are set to the square root of $S'_m(v)$ and phases are assumed to be uniform random variables in the range of $[0, 2\pi]$. A time series at each receiver s_i can then be calculated by rotating phases of $s_o(t)$ by using the array manifold Eq. (2),

$$s_i(t) = A_i(\theta, \phi)s_o(t), \tag{9}$$

where (θ, ϕ) is the desired direction of the radar system.

2) METEOR ECHOES

Meteor trail echoes are returned from ionized electrons left along the paths of meteoroids. These trails usually remain at most a second with 50 MHz and provide strong backscattering. For example, the echo power from these trails may reach 80 dB over the noise level (McKinley 1961). In radar observations of the mesosphere, successive spectra are usually averaged to reduce statistical fluctuations. This procedure is called incoherent integration. Although these meteor trails fade out in less than a second, their strong intensity contaminates the spectra severely even after the incoherent integration.

In this simulation, a meteor trail echo is modeled as a backscattering from a linearly shaped hard target with exponentially decreasing echo power that is moved by the background wind; that is, underdense meteor trail.

Phases of the meteor echo $p_i(t)$ can be calculated from the distance to each receiver $d_i(t)$. Amplitudes are the square root of the meteor echo power $P_M(t)$, which is known to decay exponentially as

$$P_M(t) = P_M(0) \exp\left[-\frac{32\pi^2 Dt}{\lambda^2}\right], \quad (10)$$

where D is the ambipolar diffusion coefficient (Ceplecha et al. 1998). We use $D \sim 1\,\mathrm{m^2\,s^{-1}}$ at 90 km. Consequently, the time series of meteor trail echoes $s_i(t)$ can be obtained as

$$s_i = P_M(t)\exp i p_i(t). \quad (11)$$

3) SIGNAL PROCESSING

After generating received signals for both atmospheric and meteor echoes, we add them together and obtain the complex time series

$$\mathbf{s}(t) = [s_1(t), s_2(t), \ldots, s_M(t)]^T \quad (12)$$

for each channel. The covariance matrix $\mathbf{R}_{xx}$ for sample number k_t is generated and updated using the following set of expressions:

$$\mathbf{R}_{xx}(0) = \mathbf{s}(0)\mathbf{s}^H(0),$$
$$\mathbf{R}_{xx}(k_t) = \gamma\mathbf{R}_{xx}(k_t - 1) + (1 - \gamma)\mathbf{s}(k_t)\mathbf{s}^H(k_t), \quad (13)$$

where $k_t = 1, 2, \ldots$ and $0 \leq \gamma < 1$ is the forgetting factor. In this simulation, we use $\gamma = 0.995$, which is the equivalent of accumulating received signals of about 1500 samples to obtain one covariance matrix. The time series of received signals $\mathbf{s}(t)$ is synthesized employing two methods to make a comparison, the NC-TA method and nonadaptive beamforming (NA-BF) method. For each renewal of the covariance matrix, an optimal weight vector $\mathbf{W}(t)$ is calculated using Eq. (6) for the NC-TA method, with $\alpha = 0$ and $M = 25$. The permissive SNR loss G_{SNR} is set as an increasing sequence of five equal intervals in the range from 0.5 to 3 dB. For the NA-BF method, $\mathbf{W}(t) = \mathbf{A}(\theta, \phi)$ using an array manifold. The desired direction (θ, ϕ) is set to $(0°, 0°)$. The beam synthesis of the received signals using the weight vector $\mathbf{W}$ is performed through Eq. (3).

4) INCOHERENT INTEGRATION

After the beam synthesis of the received signals and calculation of spectra, we perform incoherent integration by accumulating N_i successive spectra. The fluctuation of amplitudes is expected to be reduced to $1/\sqrt{N_i}$ in this manner. In practice, spectra with strong meteor clutters should be removed from the integration. We set a threshold B_t as $+3.5\,\mathrm{dB}$ over the peak power of atmospheric echo P_S for deciding which spectrum contains a clutter and should be discarded. In this simulation, the peak power of an atmospheric echo is known—for example, $+10\,\mathrm{dB}$ over the noise level. The probability of random fluctuations being at least $+3.5\,\mathrm{dB}$ over the actual peak power—for example, $+13.5\,\mathrm{dB}$ over the noise level in this case—is less than 5% in the χ^2 distribution with 2 degrees of freedom. Any peak over B_t is thus assumed to be a clutter.

b. Wind velocity estimation employing the least squares fitting method

After the incoherent integration, we estimate the mean wind velocities v_d from the averaged spectra employing the least squares fitting method (Yamamoto et al. 1988). This method fits a Gaussian spectrum $\hat{S}(k_\nu; P_S, v_d, \sigma)$ to the simulated observed spectrum $S'_m(k_\nu)$, such that the root-mean-square (RMS) of the residue

$$\epsilon = \sqrt{\frac{1}{k_\nu}\sum_{k_\nu}[\hat{S}(k_\nu; P_S, v_d, \sigma) - S'_m(k_\nu) - P_N]^2} \quad (14)$$

is minimized by changing parameters P_S, v_d, and σ. Here, k_ν is the discrete sample number of frequency components. Note that the noise level of the observed spectrum P_N must be obtained in advance employing other methods (Hildebrand and Sekhon 1974; Woodman 1985).

c. Simulation settings

1) RADAR SYSTEM

The target radar system is based on the MU radar at Shigaraki MU Observatory, Japan. Figure 2 shows the antenna position and the group number of the MU radar. The MU radar has 475 crossed Yagi antennas and the signals received from each of the 19 receivers are combined into one channel, forming an adaptive antenna with 25 channels. The radar frequency is 46.5 MHz. Observational parameters are listed in Table 1. Note that using $N_i = 38$ successive spectra for incoherent integration is equivalent to averaging over about 1 min.

2) EXPERIMENTAL PARAMETERS

We conduct two types of simulations. First, assuming an arbitrary range with both atmospheric and meteor echoes observed, we vary the SNR of the atmospheric echoes and calculate the RMS error of the wind velocity estimation at each SNR. We call this "simulation 1." In this simulation, we set the meteor clutter to have an echo intensity of $+15\,\mathrm{dB}$ over the noise level and consider a radial velocity of $+5\,\mathrm{m\,s^{-1}}$. The appearance rate of
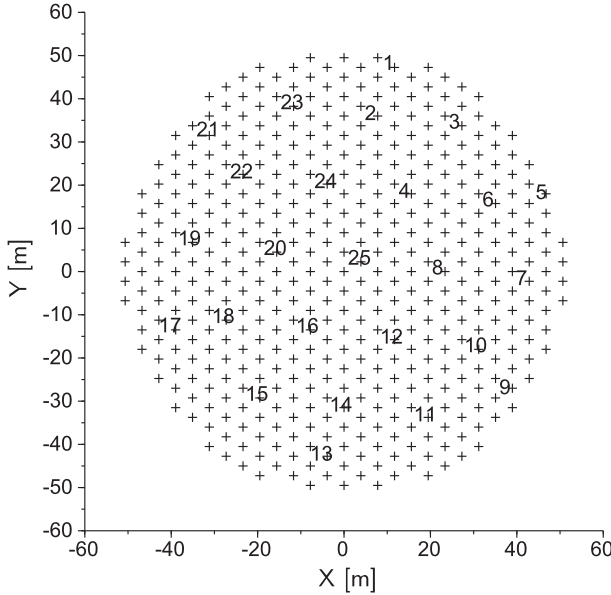
FIG. 2. Antenna position and channel number assignment for the simulation based on the MU radar.

meteor echoes is 100%— that is, each spectrum contains a meteor echo. Note this is not a realistic setting about the number of meteor trails, but this simulation is intended to test the maximum capability of the method and the more realistic situation is given to simulation 2. The SNR of the atmospheric echo is changed from 0 to +30 dB over the noise level, in steps of 5 dB. The signal-to-interference ratio (SIR) is then moved from −15 to +15 dB. We run this simulation 100 times to obtain the averaged RMS error of the wind velocity estimations. The thresholding of the contaminated spectra stated in section 3a(4) is not used in simulation 1.

Second, we apply the same procedure to multiple ranges and records, assuming actual mesosphere observations. We call this "simulation 2." Again, we generate $N_R = 100$ successive records of simulation data and average the results. The thresholding of the spectra is introduced in this simulation to conform to the actual observations. We also consider several additional variabilities. The appearance rate of the meteor echoes is 33%—that is, one-third of all spectra contain a meteor echo. The height distribution of meteor trails has a Gaussian-like form, and has a maximum at about 90 km, as stated in Nakamura et al. (1991), for example. We therefore simulate the range of each meteor using a random variable that follows a Gaussian distribution with a mean of 90 km and a standard deviation of 6.7 km. For the atmospheric echoes, decays of the echo power P_S with a range from the radar and the cyclic variations of the mean wind velocity v_d assuming a gravity wave are introduced:

TABLE 1. Radar system settings for the simulation based on standard mesospheric observations of the MU radar.

Interpulse period	$3120\,\mu s$
Time resolution	3.12 ms
Range resolution	900 m
Ranges	75–127 km
No. of time samples N_ν	128
No. of range samples N_r	59
No. of incoherent integration N_i	38
No. of total records N_R	100

$$P_S(r) = P_S^0 D_S^{|r-r_m|} \quad \text{and} \quad (15)$$

$$v_d(t) = v_d(0) + v_g \sin\left(\frac{2\pi}{T_g}\right), \quad (16)$$

where r_m is the range having maximum echo power, D_S is the decay factor for echo power, and v_g and T_g are the amplitude and wave period of the gravity wave, respectively.

Tables 2 and 3 give the detailed parameters for generating atmospheric and meteor echoes in simulation 2. Note that decibel values are against the noise level.

d. Results

Figure 3 is an example of the spectra generated in simulation 1. The horizontal axis is the Doppler velocity $(m\,s^{-1})$ and the vertical axis is the echo intensity (dB). In this case, the SNR of the atmospheric echo is set to +10 dB. The results of wind velocity estimation are also marked. Figure 4 is the RMS error in the Doppler velocity estimations for each SIR averaged 100 times, obtained by employing the NA-BF method and the NC-TA method. The horizontal axis is the SIR we tested from −15 to 15 dB, and the vertical axis is the RMS error at each SIR.

Next, Fig. 5 shows the relationship between the accuracy of wind velocity estimations and the echo intensities of the desired or undesired signals for each beam synthesis method. The left panel of Fig. 5 shows the averaged RMS error of the estimated wind velocity in simulation 2. The horizontal axis is the RMS error of the estimated Doppler velocity $(m\,s^{-1})$. The right panel shows the maximum echo intensity of the atmospheric and meteor echoes averaged in simulation 2. Here, the

TABLE 2. Parameters for generating atmospheric echoes in simulation 2.

Decay factor for ranges D_S	$-3\,dB\,km^{-1} = 0.5$
Range at the max power r_m	78 km
Max echo power $P_S^0 = P_S(r_m)$	15 dB
Spectral width	$1\,m\,s^{-1}$
Amplitude of the gravity wave v_g	$5\,m\,s^{-1}$
Wave period of the gravity wave T_g	33 min

TABLE 3. Parameters for generating meteor echoes in simulation 2.

Mean of power distribution P_0	20 dB
Std dev of power distribution σ_P	2.5 dB
Mean of range distribution	90 km
Std dev of range distribution	6.7 km
Appearance rate	33%
Radial velocity	0–25 m s^{-1}
Diffusion coefficient D	1.0 m^2 s^{-1}
Orientation	Uniformly random

atmospheric echo has a peak power around 78 km, while the intensity of meteor echoes increases with range. The vertical axes of the two panels have units of kilometers.

e. Discussion

In simulation 1, all spectra are used without thresholding. In such a case, the adaptive meteor clutter rejection technique is found to improve the accuracy of the wind velocity estimations, especially when the interference is stronger than or almost equal to the atmospheric echoes. As seen in Fig. 3, the meteor clutter is suppressed well by the NC-TA method. Thus, wind velocities are estimated near the true peak by the NC-TA method, while the NA-BF method gives wrong values contaminated by meteor clutters. Consequently, Fig. 4 shows that with SIRs under 0 dB, as in Fig. 3, the echo intensity of meteor clutters is stronger than that of atmospheric echoes and the NA-BF method gives incorrect estimations of wind velocity because of the interference. As a result, the observable echo intensity improves by about 15 dB when employing the NC-TA method. In addition, we should mention that meteor trail echoes can be extracted by employing the same method if needed, by simply subtracting the obtained meteor-suppressed signals from the original received ones.

In simulation 2, strong interference is suppressed by spectral thresholding. Employing this procedure, the initial guess of the peak search is made accurate to some extent by discarding contaminated spectra in incoherent integration, while fewer spectra result in more fluctuation in the integrated spectra, which can bring low accuracy. Additionally, interferences below the threshold remain with no change with the NA-BF method, and this leads to an increase in the RMS error in the spectral fitting for the NA-BF method. On the contrary, the NC-TA method suppresses interferences automatically in advance, and improves both the number of spectra discarded in incoherent integration and the RMS error in the spectral fitting. These trends are clearly shown in Fig. 5. Here, the NC-TA method discards only 1.3% of spectra, while 10.9% with the NA-BF method. The average RMS errors at 78 km are 1.5 m s^{-1} for the NC-TA method and 10.1 m s^{-1} for the NA-BF method. As seen
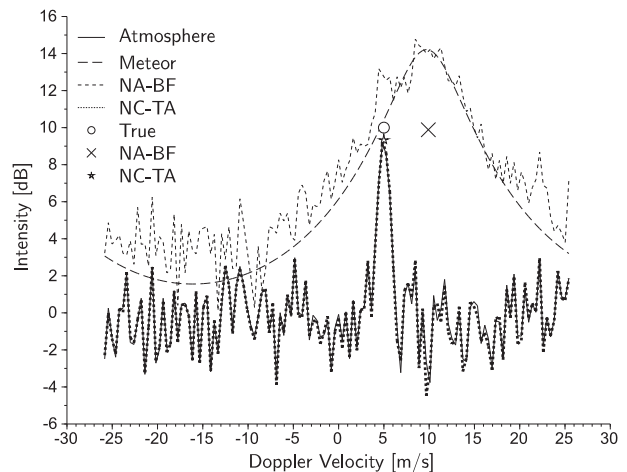
FIG. 3. Example of the spectra generated in simulation 1. The SNR of the atmospheric echo is +10 dB. Lines are the spectra of the atmosphere only, meteor only, and the synthesized spectra of the NA-BF method and the NC-TA method. Marks show the actual peak powers and Doppler velocities and the peak powers and Doppler velocities estimated employing the NA-BF method and the NC-TA method.

in Fig. 5b, the average SIR of simulation 2 is at most −10 dB at 78 km. Figure 4 shows that even the NC-TA method gives low accuracy with the SIR under −10 dB and thus the result is consistent with simulation 1. At higher ranges, where there are more meteor echoes, the accuracy of the estimated wind velocity is low for both methods, but the error is about 8 m s^{-1} less for the NC-TA method. Additionally, the RMS error has a flat floor from 76 to 78 km with the NC-TA method, which is about 4 times as wide as that with the NA-BF method. This is the benefit of the adaptive clutter rejection
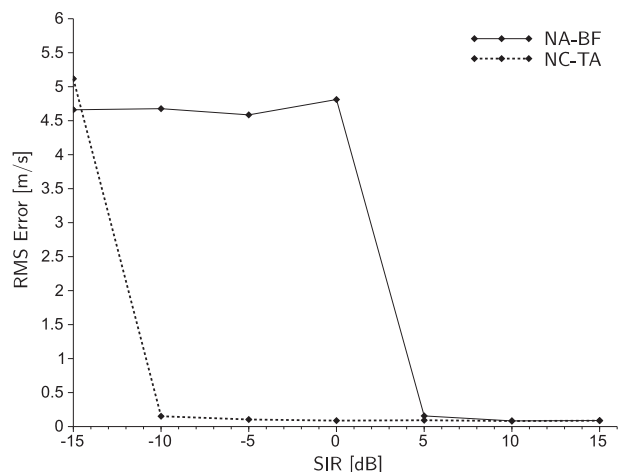
FIG. 4. RMS error of wind velocity estimated with the NA-BF method and the NC-TA method. The horizontal axis is the SIR and the vertical axis is the RMS error between the true velocity and the estimated velocity.
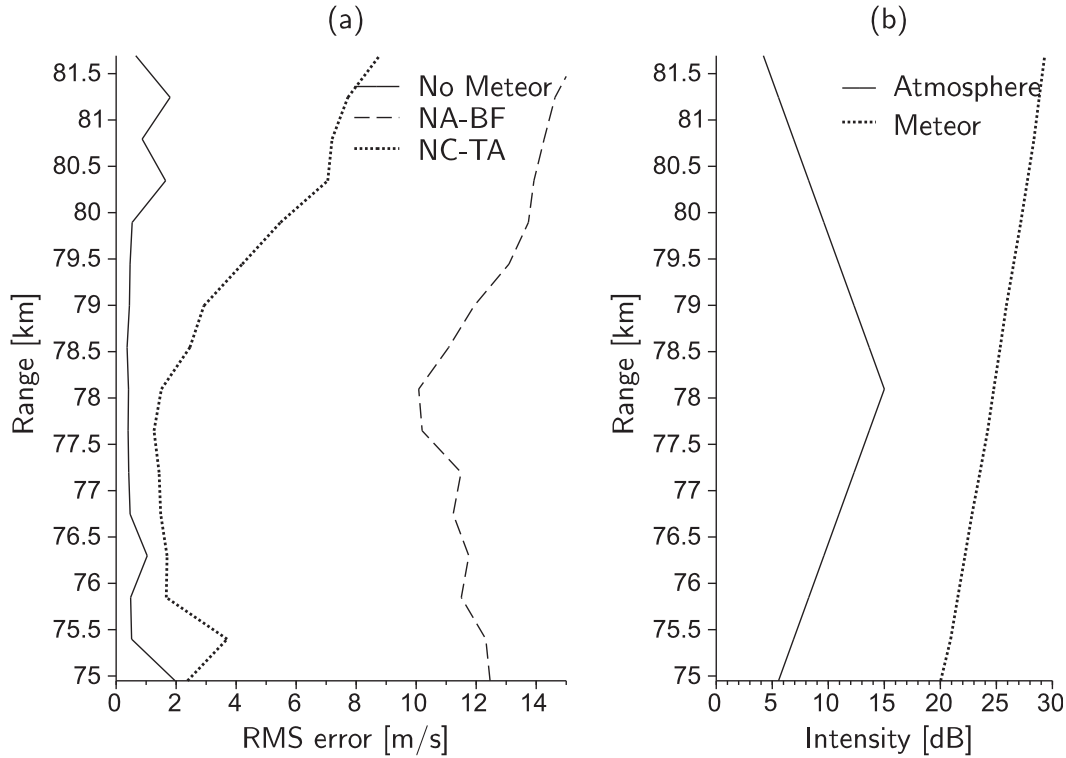
FIG. 5. (a) RMS errors of the wind velocity estimations of the NA-BF method and the NC-TA method. The ordinate has a unit of kilometers. (b) Intensities of the atmospheric and meteor echoes for each range.

technique and implies the effectiveness of the technique in mesosphere observations.

4. Applying the adaptive meteor clutter rejection technique to an actual observation

This section presents results of applying the adaptive meteor clutter rejection technique to actual mesospheric observations.

a. Observational settings of the radar system

A series of meteor observations was made on 8 October 2011 at Shigaraki MU Observatory. We use $N_R = 100$ successive records taken from 1405 to 1546 UTC. The observational parameters are listed in Table 4. As done in simulation 2 of section 3, the time resolution of the adaptive beam synthesis is 3.12 ms. After the clutter cancellation, $N_i = 38$ successive spectra are used for incoherent integration to obtain each record, which is equivalent to averaging over about 1 min.

b. Signal processing

We apply the NA-BF method and the NC-TA method to the same observed data sequence to compare the ability of the two methods to suppress clutter. Procedures of the signal processing are exactly the same as

those described in section 3. Additionally, thresholding and accumulation of spectra are performed as in the previous section. However, the threshold B_t for removing contaminated spectra is unknown for the actual observation, and we determine it as follows. First, we perform adaptive beam synthesis on all received signals, employing the NA-BF method and the NC-TA method, and then convert them into spectra by taking the Fourier transform to obtain synthesized spectra $S(k_T, k_\nu)$, where $k_T = 1, \dots, N_i \times N_R$ is the spectrum index and $k_\nu = 1, \dots, N_\nu$ is the frequency component index. We then take the frequency-wise sum of $S(k_T, k_\nu)$ as

$$\hat{S}(k_T) = \sum_{k_\nu = 1}^{N_\nu} S(k_T, k_\nu). \qquad (17)$$

TABLE 4. Radar system settings for the observation made by the MU radar from 1405 to 1546 UTC 8 Oct 2011.

Interpulse period	$3120\,\mu s$
Time resolution	3.12 ms
Range resolution	900 m
Valid ranges	75–127 km
No. of time samples N_ν	512
No. of range samples N_r	59
No. of incoherent integration N_i	38
No. of total records N_R	100
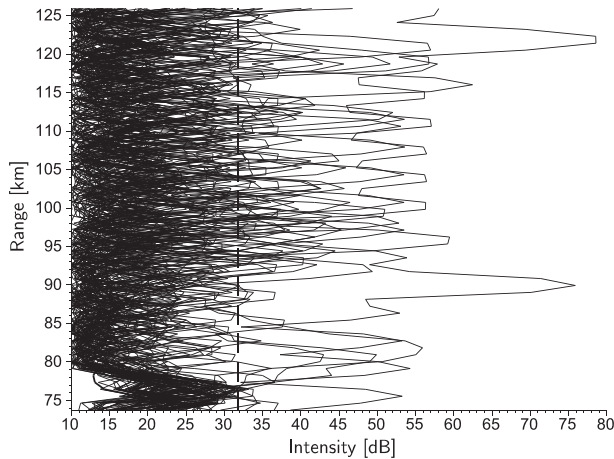
FIG. 6. Peaks of spectra processed by the NA-BF method for each range overlaid throughout the observation period on 8 Oct 2011. The horizontal axis is the peak power for each range (dB) and the vertical axis is the range (km). The dashed line is the threshold B_t we selected.

FIG. 7. As in Fig. 6, but processed with the NC-TA method.

Finally, we choose the threshold B_t to satisfy the relation

$$p[\hat{S}(k_T) > B_t] \leq 5\% \qquad (18)$$

at ranges of 74–80 km. Here, $p[\hat{S}(k_T) > B_t]$ is the probability of peaks in $\hat{S}(k_T)$ being larger than the current threshold B_t. The objective of Eq. (18) is to make the number of discarded spectra the same as in the simulation of the previous section. To compute B_t, we iteratively enlarge B_t to find the minimum value that satisfies Eq. (18). The overlaid spectral peaks are shown in Figs. 6 and 7 for the NA-BF method and the NC-TA methods, respectively. The horizontal axis is the peak power for each range (dB) and the vertical axis is the range (km). Dashed lines are the threshold B_t for the spectra processed by the two methods.

c. Results

Table 5 gives the threshold B_t we selected for removing spectra with contaminations, the defection ratio Φ_D in the incoherent integration, and the equivalent number of incoherent integration η. Figure 8 shows the average errors of the wind velocity estimation versus the range (74–84 km) estimated from spectra processed with the NA-BF method and the NC-TA method. Thin lines are biased by the standard deviation σ for each range.

d. Discussion

1) COMPARISON OF THE DEFECTION RATIO

Table 5 shows that the NC-TA method discards only about one-third of the spectra discarded by the NA-BF

method through thresholding in incoherent integration. Additionally, comparing Figs. 6 and 7, it is clear that the number of peaks in spectra processed by the NC-TA method that are considered to be meteor clutters is much less than that in the case of the NA-BF method. The average suppression ratio of meteor clutters is nearly 15 dB, which is the same result as for simulation 1 in section 3.

2) DIFFERENCES IN WIND VELOCITY ESTIMATION

As seen in Fig. 8, the standard deviations of the average wind velocities at ranges of 78–80 km and 73.7 km estimated with the NC-TA method are much lower than those estimated with the NA-BF method. These ranges are considered to be the boundary regions where atmospheric echoes are weak and meteor clutters are dominant. However, the NC-TA method works for both clutter suppression and decreasing fluctuations of spectra and these benefits lead to observable ranges that are almost twice as wide.

5. Summary and conclusions

This paper presented the result of applying an adaptive meteor clutter rejection technique to an actual mesosphere observation.

TABLE 5. Threshold B_t for discarding contaminated spectra in incoherent integration, the defection ratio Φ_D with thresholding, and the equivalent number of incoherent integration η for the observation.

	BF	NC-TA
B_t	31.4 dB	28.6 dB
Φ_D	13.5%	4.37%
η	$\simeq$32.9	$\simeq$36.3
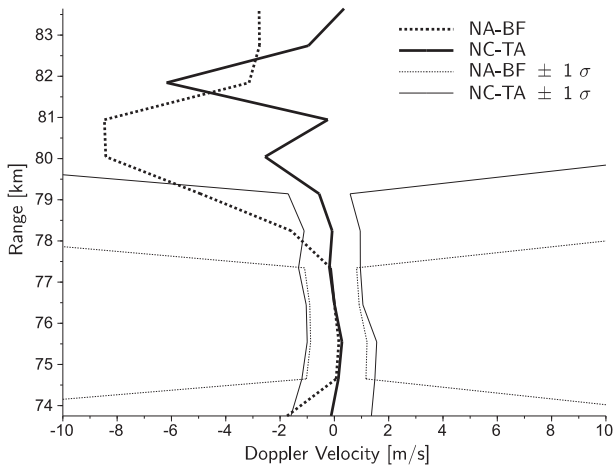
FIG. 8. Average RMS errors in wind velocity estimation for each range calculated with the NA-BF method and the NC-TA method. Thin lines are biased by $\pm1\sigma$.

In section 3, we presented the results from two simulations. First, we examined the capability of the NC-TA method to suppress contaminations. The NC-TA method reproduced the desired signals with the SNRs exceeding $+5$ dB (SIR of -5 dB), which is an improvement of $+15$ dB compared with the result of the ordinary nonadaptive beamforming method. Second, we performed a more realistic simulation of a mesosphere observation. In this case, the method estimates the wind velocity with an RMS error of about 1.5 m s^{-1} with an SIR of -10 dB, and the spectral fitting was successful for ranges 4 times as wide as in the case of the nonadaptive beamforming method.

In section 4, the NC-TA method was applied to an actual observation made on 8 October 2011. The proposed method suppressed meteor clutters by about 15 dB on average, and the number of spectra discarded through spectral thresholding in incoherent integration with the NC-TA method was about one-third of the number for the nonadaptive beamforming method. Additionally, the standard deviation of the wind velocity estimation was less than 2 m s^{-1} for ranges twice as wide

as those for the conventional method—that is, the observable range doubled.

The above-mentioned simulation and observational results show that the NC-TA method is a good solution for mesosphere observations contaminated by meteor clutters.

REFERENCES

Ceplecha, Z., J. Borovička, W. G. Elford, D. O. ReVelle, R. L. Hawkes, V. Porubčan, and M. Šimek, 1998: Meteor phenomena and bodies. *Space Sci. Rev.,* **84,** 327–471, doi:10.1023/A:1005069928850.

Hildebrand, P. H., and R. Sekhon, 1974: Objective determination of the noise level in Doppler spectra. *J. Appl. Meteor.,* **13,** 808–811, doi:10.1175/1520-0450(1974)013<0808:ODOTNL>2.0.CO;2.

Kamio, K., K. Nishimura, and T. Sato, 2004: Adaptive sidelobe control for clutter rejection of atmospheric radars. *Ann. Geophys.,* **22,** 4005–4012, doi:10.5194/angeo-22-4005-2004.

McKinley, D. W. R., 1961: *Meteor Science and Engineering.* McGraw-Hill Series in Engineering Sciences, McGraw-Hill, 309 pp.

Nakamura, T., T. Tsuda, M. Tsutsumi, K. Kita, T. Uehara, S. Kato, and S. Fukao, 1991: Meteor wind observations with the MU radar. *Radio Sci.,* **26,** 857–869, doi:10.1029/91RS01164.

Nishimura, K., T. Nakamura, T. Sato, and K. Sato, 2012: Adaptive beamforming technique for accurate vertical wind measurements with multichannel MST radar. *J. Atmos. Oceanic Technol.,* **29,** 1769–1775, doi:10.1175/JTECH-D-11-00211.1.

Takao, K., and N. Kikuma, 1986: Tamed adaptive antenna array. *IEEE Trans. Antennas Propag.,* **34,** 388–394, doi:10.1109/TAP.1986.1143821.

——, M. Fujita, and T. Nishi, 1976: An adaptive antenna array under directional constraint. *IEEE Trans. Antennas Propag.,* **24,** 662–669, doi:10.1109/TAP.1976.1141411.

Tsuda, T., M. Yamamoto, T. Sato, S. Kato, and S. Fukao, 1985: Comparison observations between the MU radar and the Kyoto meteor radar. *Radio Sci.,* **20,** 1241–1246, doi:10.1029/RS020i006p01241.

Wang, Z., J. Li, and P. Stoica, 2003: Comparison between norm constrained and robust capon beamformers. *IEEE International Symposium on Phased Array Systems and Technology 2003,* IEEE, 170–175.

Woodman, R. F., 1985: Spectral moment estimation in MST radars. *Radio Sci.,* **20,** 1185–1195, doi:10.1029/RS020i006p01185.

Yamamoto, M., T. Sato, P. May, T. Tsuda, S. Fukao, and S. Kato, 1988: Estimation error of spectral parameters of mesosphere-stratosphere-troposphere radars obtained by least squares fitting method and its lower bound. *Radio Sci.,* **23,** 1013–1021, doi:10.1029/RS023i006p01013.